sustainability

MDPI

Article

Mapping Soil Erosion Potential in Algeria's Wadi Mina Basin: Insights from Revised Universal Soil Loss Equation and Geographic Information System for Sustainable Land Management

Mohammed Achite [1,2], Pandurang Choudhari [3], Abderrezak Kamel Toubal [1], Tommaso Caloiero [4,*], Alessandra De Marco [5] and Sylvain Ouillon [6,7]

1 Water and Environment Laboratory, Faculty of Nature and Life Sciences, Hassiba Benbouali University of Chlef, Chlef 02180, Algeria; m.achite@univ-chlef.dz (M.A.); a.toubal@univ-chlef.dz (A.K.T.)
2 Georesources, Environment and Natural Risks Laboratory, University of Oran 2 Mohamed Ben Ahmed, Oran 31000, Algeria
3 Department of Geography, University of Mumbai, Mumbai 400032, India; choudharipp79@gmail.com
4 National Research Council of Italy, Research Institute for Geo-Hydrological Protection (CNR-IRPI), 87036 Rende, Italy
5 National Research Council of Italy, Territorial Research Area of Cosenza, 87036 Rende, Italy; alessandra.demarco@cnr.it
6 Laboratory of Space Geophysical and Oceanographic Studies (LEGOS), CNES, CNRS, IRD, UT3, University of Toulouse, 31013 Toulouse, France; sylvain.ouillon@legos.obs-mip.fr
7 Department of Water—Environment—Oceanography, University of Science and Technology of Hanoi, Vietnam Academy of Science and Technology, Hanoi 100000, Vietnam
* Correspondence: tommaso.caloiero@cnr.it; Tel.: +39-0984-841-464

Abstract: In this paper, the Revised Universal Soil Loss Equation (RUSLE) model has been employed as a critical analytical instrument to assess the likelihood of soil erosion and pinpoint the most appropriate locations for conservation initiatives in the Wadi Mina basin (Algeria). The compilation of thematic maps was accomplished through the integration of the Spatial Analyst module in ArcGIS, resulting in a comprehensive map depicting potential erosion. This process incorporated rainfall data collected over a four-decade period from 1971 to 2010. The findings of this study demonstrate that the intensity of soil erosion and the generation of sediment are influenced by the topographical characteristics of the region, and the steepness of the terrain. Soil erosion within the Wadi Mina basin presents notable fluctuations, spanning a spectrum from a low of 0 to a high of 772.16 tons per hectare annually, with the mean annual erosion rate calculated at 16.69 tons per hectare. The Sediment Delivery Ratio (SDR) for the basin is estimated to be around 19.20%. Understanding soil erosion patterns at different sub-basin levels can be valuable for designing effective conservation strategies. This information helps to implement erosion control measures and to improve overall environmental management within the basin.

Keywords: soil erosion; RUSLE; Wadi Mina basin; Algeria; GIS; land management

Academic Editor: Liying Sun

Received: 13 March 2025
Revised: 20 May 2025
Accepted: 29 May 2025
Published: 30 May 2025

Citation: Achite, M.; Choudhari, P.; Toubal, A.K.; Caloiero, T.; De Marco, A.; Ouillon, S. Mapping Soil Erosion Potential in Algeria's Wadi Mina Basin: Insights from Revised Universal Soil Loss Equation and Geographic Information System for Sustainable Land Management. *Sustainability* **2025**, *17*, 5038. https://doi.org/10.3390/su17115038

1. Introduction

Soil erosion poses a multifaceted environmental concern with far-reaching implications. This phenomenon contributes to soil degradation and depletion, affecting land fertility and crop yields. Moreover, it accelerates reservoir sedimentation, thereby diminishing water storage capacity crucial for irrigation, hydroelectric power generation, and flood control. The erosion process also compromises soil infiltration capabilities and influences

the movement and ecological impact of contaminants, potentially jeopardizing wildlife habitats and water resources essential for domestic, agricultural, and industrial applications. In severe instances, soil erosion emerges as a pivotal factor driving the desertification of semi-arid landscapes. For soil erosion estimation, different kinds of models and methodologies exist. These range from simple to more complex approaches, encompassing empirical or conceptual models as well as physically based ones. The various models require diverse types of input data and differ in their ability to forecast soil erosion caused by hydrological factors [1,2].

In data-scarce environments, empirical models are widely employed due to their simplicity and minimal requirements for data and parameters. Notable examples include USLE [3], updated version RUSLE [4], RMMF [5], and EPM [6]. Conversely, physically based models simulate the primary mechanisms involved in erosion processes, adhering to mass and energy conservation principles. These comprise ANSWERS [7], CREAMS [8], KINEROS2 [9], EUROSEM [10], EPIC [11], WEPP [12], and PESERA [13]. Conceptual models, like AGNPS [14], LASCAM [15], and SWAT [16], integrate aspects of both physically based and empirical approaches. It is important to note that these models vary in their simulation scope; some focus solely on gross erosion or partial gross erosion, while others incorporate both land erosion and hydrologic network transport models, including erosion and deposition processes. For comprehensive reviews of erosion models, readers may refer to recent publications by De Vente et al. [17], Dutta [18], and Batista et al. [19].

The RUSLE, proposed by Renard et al. [4] as an advancement to the original Universal Soil Loss Equation (USLE) developed by Wischmeier [3], is one of the most widely utilized empirical approaches for assessing soil erosion rates in this model. These models are constrained to forecasting the typical rates of sheet and rill erosion while failing to incorporate the impact of gully erosion. Contemporary advancements in geographic information technology have bolstered traditional methodologies, offering sophisticated tools for resource control, analysis, and management. The factors utilized in RUSLE for erosion evaluation can be readily incorporated into a spatial framework for soil loss prediction. Digital Elevation Models (DEMs) and remote sensing data enable efficient and comprehensive assessments of erosion threats. The availability of soil erosion data at various sub-basin scales facilitates the implementation of localized or distributed conservation strategies aimed at erosion prevention, regulation, and overall enhancement of environmental management within the basin. The RUSLE model has been extensively employed in recent years to assess soil erosion across various geographical scales. Numerous global studies have utilized this model, including research by Azaiez [20] and Panagos et al. [21]. Additionally, investigations have been conducted at both territorial [22] and basin scales [23,24]. In the North African context, specifically in Tunisia [25,26], Morocco [27,28] and Algeria [29–39], researchers have applied RUSLE to quantify soil loss across diverse basins and climatic conditions.

The Wadi Mina basin has been the subject of numerous investigations focusing on erosion and sediment transport assessment [40]. A significant contribution to this field was made by Achite and Meddi [41], who developed a statistical methodology to quantify sediment yield at various gauging locations within the basin. This research concentrated on five upstream sub-basins of the Sidi Me Hamed Ben Aouda dam, drawing upon data amassed over a 22-year interval from 1973 to 1995. Preliminary findings, derived from the sediment rating curve technique, revealed that the Oued Haddad basin experiences more severe degradation than its counterparts, exhibiting a specific degradation rate of 212 $t/km^2/year$. This particular site serves as a clear indicator of soil depletion. A steep topography and an inconsistent vegetation cover, which fail to provide adequate land protection, exacerbate the area's vulnerability to erosion.

The basin under consideration shows a degradation rate inferior to that of the Oued Haddad basin (D = 191 t/km^2/year). The Oued El Abd basins at Ain El Hamara station exhibit a specific degradation of approximately 117 t/km^2/year, while at Takhmaret station, this value is reduced to roughly 65 t/km^2/year. The Wadi Mina at the Sidi Mohamed Ben Aouda dam is estimated to cause a specific degradation of 187 t/km^2/year. Research conducted by Benchettouh et al. [29] utilized thematic maps of various erosive factors, based on the RUSLE and implemented in GIS using ArcGIS 10.2 software, to delineate erosive risk areas in the basin. This approach yielded a reliable assessment of annual soil loss rates. The assessment of erosion categories revealed a range of potential soil loss rates, from negligible to over 100 metric tons per hectare per year, with an average projected annual soil erosion of 11.2 t/ha/year. Approximately half of the basin was found to have from very low to low risk of erosion, exhibiting soil loss values between 0 and 7.4 t/ha/year. Additionally, regions with a moderate erosion risk, characterized by soil loss rates of 7.4 to 12 t/ha/year, accounted for more than 13.9% of the basin. These findings hold significant implications for the selection and implementation of effective soil and water conservation strategies in areas deemed highly susceptible to water-induced erosion.

A methodological approach was presented by Hallouz et al. [42] to investigate the sources and current state of sediment deposition within the Sidi M'Hamed Ben Aouda Dam, situated in the northwest region of Algeria. Their approach incorporated hydro-fluviometric techniques and specific attributes of Wadi Mina. The analysis encompassed liquid discharge data over a 41-year timeframe (1969–2010), while solids and suspended sediment concentration data spanned variable periods ranging from 22 to 40 years across the catchment area. Pluviometric investigations examined rainfall patterns over 77 years (1930–2007). Statistical analyses of historical precipitation and discharge series revealed a significant decline in rainfall exceeding 20% across the entire basin since 1970. The progression of solids input was quantified, with the highest values noted. This study analyzes yearly soil erosion rates in the Mina basin, located in northwestern Algeria, by employing geospatial techniques combined with the RUSLE model. The research aims to contribute to the formulation of effective strategies for soil and water conservation, particularly in areas highly vulnerable to significant water-induced erosion.

2. Study Area and Data

The Wadi Mina basin, a geographic subdivision of the larger Wadi Cheliff basin, encompasses an area of approximately 4900 square kilometers. Located in the northwestern region of Algeria, the basin's geographic boundaries are defined by the coordinates of longitudes 00°22′59″ E and 01°09′02″ E and latitudes 34°41′57″ N and 35°35′27″ N (Figure 1).

The Wadi Mina basin is fed by four main tributaries: Wadi Taht, Wadi Haddad, Wadi Mina, and Wadi Abd. The region features a diverse and rugged landscape, with elevation levels varying from 164 meters to 1327 meters above sea level. Moreover, according to the division already drawn up by the National Water Resources Agency (ANRH), the Mina catchment area is made up of five sub-catchment areas drained by secondary wadis of varying lengths from one sub-catchment area to another. These main wadis are the Oued Mina at the Oued Abtal hydrometric station (4126 km^2), the Oued Haddad at the Sidi Abdelkader Djillali station (470 km^2), the Oued Taht at the Kef Mehboula station (680 km^2), the Oued Abd at the Takhmaret station (1553) and the Ain Hamara station (2480 km^2) and the entire basin (4900 km^2) at the Sidi Mhamed Ben Aouda dam (SMBA). The morphometric, topographic and hydrographic characteristics of the five sub-catchment areas and the Mina catchment area at the dam are shown in Table 1.

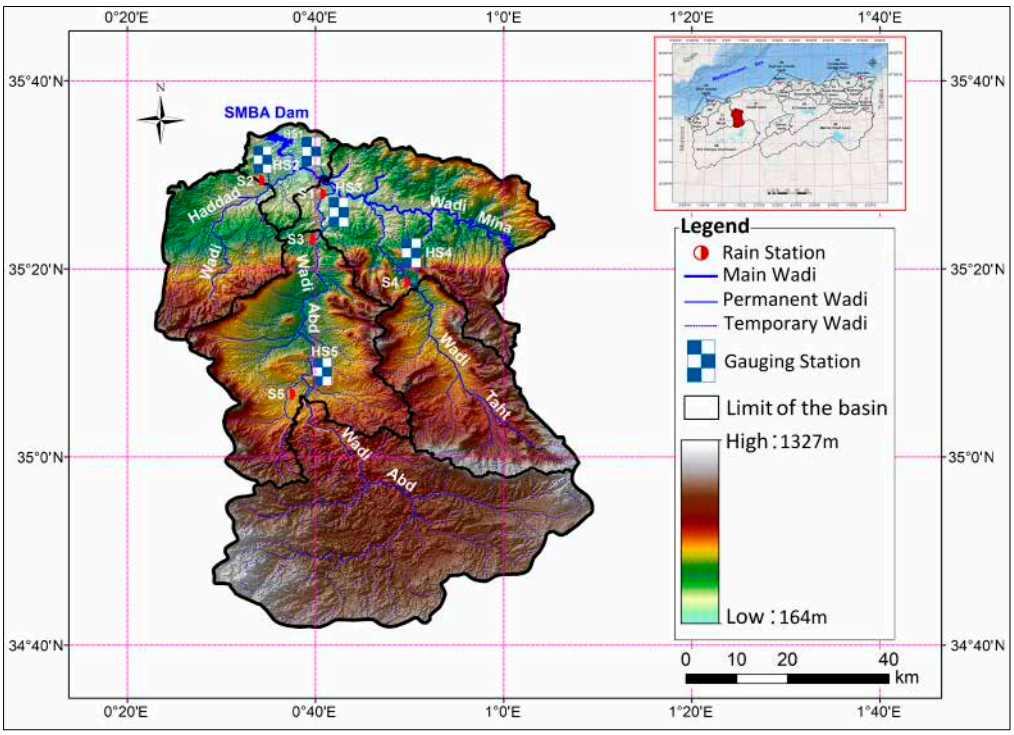

Figure 1. Location and map of the elevation within the Wadi Mina basin.

Table 1. Main characteristics of the investigated sub basins in the Mina basin.

Type	Parameters	Symbol	Unit	SB 01	SB 02	SB 03	SB 04	SB 05	Entire Basin
Morphometric characteristics	Area	(S)	Km^2	4126.00	480.00	2480.00	680.00	1553.00	4900.00
	Perimeter	(P)	Km	330.44	106.00	295.61	139.40	218.60	343.30
	Gravelius compactness index	(Kc)		1.44	1.35	1.66	1.50	1.55	1.37
	Length of equivalent rectangle	(L)	Km	133.03	41.22	127.27	57.35	91.56	136.76
	Width of equivalent rectangle	(l)	Km	31.01	11.40	19.49	11.86	16.96	34.86
Topographical characteristics	Maximum altitude	(Hmax)	m	1156.00	1156.00	1327.00	1242.00	1327.00	1327.00
	Minimum altitude	(Hmin)	m	230.00	230.00	283.00	494.00	625.00	164.00
	Average altitude	(Hmean)	m	815.63	645.86	891.28	861.90	983.57	771.50
	Median altitude	(H50%)	m	755.00	800.00	650.00	950.00	1000.00	790.00
	Altitude at 5% of the surface	(H5%)	m	1200.00	1100.00	1200.00	1185.00	1285.00	1165.00
	Altitude at 95% of the surface	(H95%)	m	400.00	250.00	400.00	600.00	685.00	375.00
	Global slope index	(Ig)	m/km	6.01	20.62	6.29	10.20	6.55	5.88
	Specific elevation	(Ds)	m	386.27	447.03	313.03	266.00	258.23	408.18
Hydrological characteristics	Drainage density	(Dd)	Km/Km^2	0.42	0.31	0.30	0.32	0.28	4.14
	Length of the main wadi Wadi station	(L_{mw})	Km	56.00	32.00	79.00	40.00	35.50	159.60
	Concentration time	(Tc)	Hours	17.61	8.26	16.10	10.70	13.92	25.83

The region exhibits a continental climate characterized by pronounced seasonal variations, including cold winters and scorching summers. Rainfall averages between 250 mm and 500 mm annually, with the majority occurring between November and March. The average annual temperature ranges from 16 °C to 19.5 °C. Vegetation occupies a significant portion of the basin, with the land use distribution comprising 32% scrubland, 35.8% forests, and areas dedicated to cereal cultivation [43]. The study utilized precipitation and runoff data sourced from the National Water Resources Agency (ANRH). Monthly observations spanning four decades (1970/71-2009/10) were collected from sixteen rainfall monitoring stations (Table 2 and Figure 1).

Table 2. Attributes of the precipitation measurement stations.

Station	ID	Name	Longitude (°)	Latitude (°)	Elevation (m)
S1	12702	Rahuia	1°00′	35°31′	650
S2	13001	Kef Mahboula	0°49′	35°18′	475
S3	13002	Frenda	1°01′	35°04′	990
S4	13004	Ain El Haddid	0°51′	35°04′	829
S5	13101	Mechra Safa	1°02′	35°23′	655
S6	13102	Djilali Benamar	0°49′	35°27′	300
S7	13201	Ain Kermes	1°05′	34°55′	1162
S8	13202	Rosfa	0°49′	34°54′	960
S9	13203	Tiricine	0°32′	34°54′	1070
S10	13204	Sidi Youcef	0°33′	34°48′	1100
S11	13302	Ain Hamara	0°39′	35°23′	288
S12	13304	Takmaret	0°37′	35°06′	655
S13	13306	Oues El-Abtal	0°40′	35°28′	354
S14	13401	Sidi A.E.K Djilali	0°34′	35°29′	225
S15	13407	El Hachem	0°28′	35°23′	417
S16	13410	SMBA	0°35′	35°34′	145

For topographic evaluation, the researchers accessed the 30 m Shuttle Radar Topographic Mission (SRTM) DEM data from the United States Geological Survey (USGS) website (http://earthexplorer.usgs.gov/). Furthermore, a Landsat-5 satellite image captured on 14 September 2009, was utilized to map the NDVI (Normalized Difference Vegetation Index) and compute the C factor. Soil data were retrieved from the Harmonized World Soil Database version 1.2 (http://www.fao.org).

The slope maps were prepared using DEM data (Figure 2) and comprised 54.55% of relatively low slopes (0–3%) and 40.53% of moderate slopes (3–12.5%) (Table 3). The central segment of the basin, spanning from east to west, exhibits pronounced gradients ranging from 12.5% to 25%, occupying approximately 4.68% of the total area and presenting considerable potential for erosion. Additionally, regions with slopes exceeding 25% constitute a mere 0.08% of the basin's surface area and are predominantly concentrated in the central and northeastern sectors [30].

Table 3. Distribution of slope classes in the Mina Wadi basin.

Classes (%)	Area (km^2)	Area (%)
0–3	2672.95	54.55
3–12.5	1985.97	40.53
12.5–25	229.32	4.68
>25	3.92	0.08
Water bodies	7.84	0.16

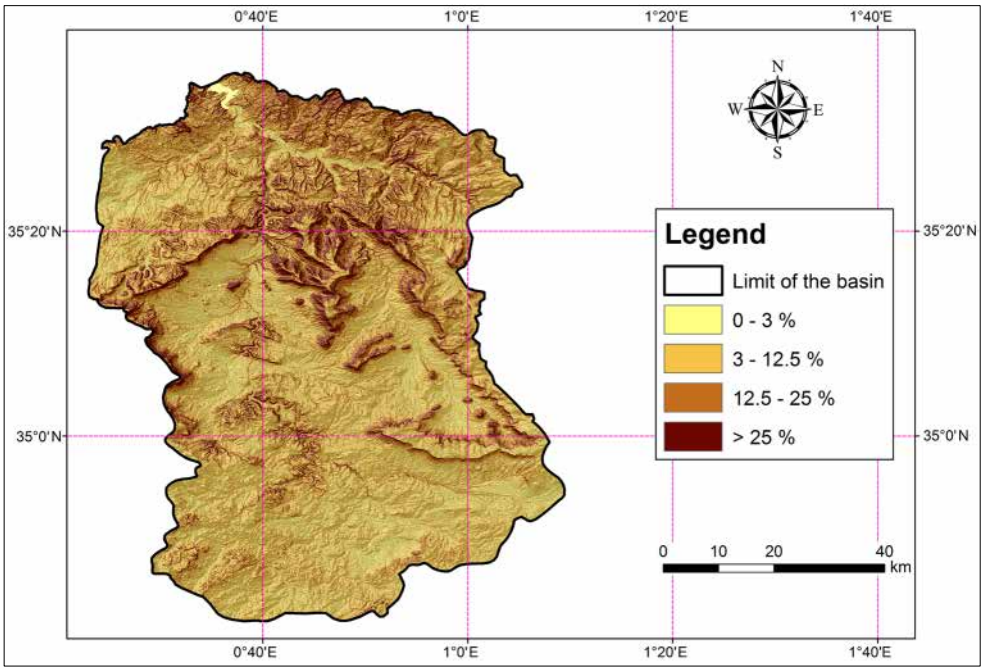

Figure 2. Slope map of the Wadi Mina basin.

The maximum annual average precipitation of 396.42 mm was recorded at Frenda station (station S3 in Figure 3 and Table 1), while the minimum average value of 218.40 mm was observed at Rosfa station (station S8, Figure 3a). The annual average maximum daily precipitation also ranged from the highest value of 35.57 mm at Frenda to a minimum of 20.65 mm at Rosfa (Figure 3b).

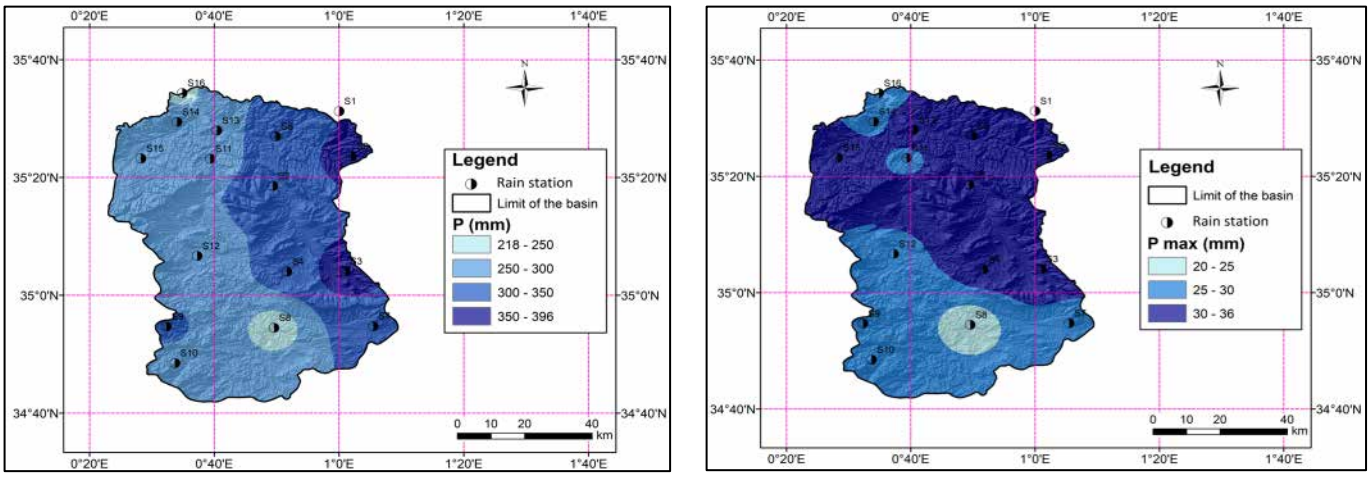

(**a**) (**b**)

Figure 3. The spatial distribution of (**a**) yearly precipitation based on the station-scale average annual precipitation and (**b**) daily peak rainfall across the study region exhibits notable variation.

The statistical measures, including the minimum, maximum, mean, standard deviation, coefficient of variation, kurtosis, and skewness for the annual rainfall (P′ in mm per year) and the annual maximum daily precipitation (d in mm per day), are presented in Table 4. These data are useful for calculating the erosivity factor of rain (factor R of the RUSLE model).

Table 4. Quantitative measures of the data employed in the analysis.

Stations	Min		Max		Mean		SD		Cv		Cs		Ck	
	P′	d	P′	d	P′	d	P′	d	P′	d	P′	d	P′	d
S1	210.00	13.40	524.70	71.60	352.53	34.39	89.27	16.18	25.32	47.05	−0.87	0.85	0.19	−0.13
S2	143.00	7.80	672.20	63.60	343.63	33.88	106.90	12.83	31.11	37.87	1.06	0.23	0.88	0.13
S3	221.00	17.00	672.90	60.20	396.42	35.57	112.03	10.58	28.26	29.76	0.09	0.62	0.61	−0.13
S4	194.80	15.40	610.00	67.00	312.83	31.77	102.92	10.43	32.90	32.84	1.60	1.30	1.23	2.54
S5	197.70	17.50	734.40	61.00	378.03	35.47	119.22	9.56	31.54	26.95	1.02	0.06	0.88	−0.02
S6	158.60	16.17	645.10	56.20	345.38	33.32	120.84	9.37	34.99	28.11	0.15	0.02	0.75	−0.49
S7	155.70	13.00	580.20	66.00	323.70	28.08	107.93	10.21	33.34	36.35	0.25	1.31	0.83	3.42
S8	77.70	7.10	557.00	71.40	218.40	20.65	113.76	11.82	52.09	57.23	2.18	2.35	1.55	7.90
S9	115.20	23.90	561.50	44.00	306.84	28.64	104.40	3.85	34.02	13.43	0.11	2.04	0.54	6.20
S10	159.20	12.00	631.00	72.80	294.89	29.01	99.59	12.71	33.77	43.80	1.76	0.97	1.15	1.95
S11	164.80	16.00	506.40	58.00	265.10	28.13	74.97	9.06	28.28	32.20	3.13	1.45	1.51	3.09
S12	120.50	11.80	413.10	49.70	254.25	29.26	73.14	9.39	28.77	32.09	−0.34	0.18	0.57	−0.67
S13	129.60	15.27	558.00	93.25	278.65	36.00	84.84	17.88	30.45	49.67	2.12	1.50	1.18	2.18
S14	135.60	11.80	474.20	43.60	254.13	28.61	72.12	8.82	28.38	30.82	1.33	−0.31	1.08	−0.99
S15	152.60	15.10	517.00	75.30	291.01	32.75	78.85	12.63	27.10	38.57	0.21	1.25	0.57	2.14
S16	141.00	10.20	436.60	40.00	237.97	26.45	63.09	7.66	26.51	28.95	1.86	−0.46	1.15	−0.37

The lithological composition of the Wadi Mina basin at the SMBA encompasses a geological sequence extending from the Primary to the Quaternary periods (Figure 4, Table 5). Within this area, Quaternary deposits are found in topographic lows and valley depressions, constituting 4.61% of the total surface area. Pliocene outcrops are extensively distributed across the northern portion of the catchment, oriented in an east–west direction, and account for 4.60% of the area. The predominant geological feature, however, is the Jurassic formations, characterized by gray–green marl, which cover approximately 68.11% of the study region.

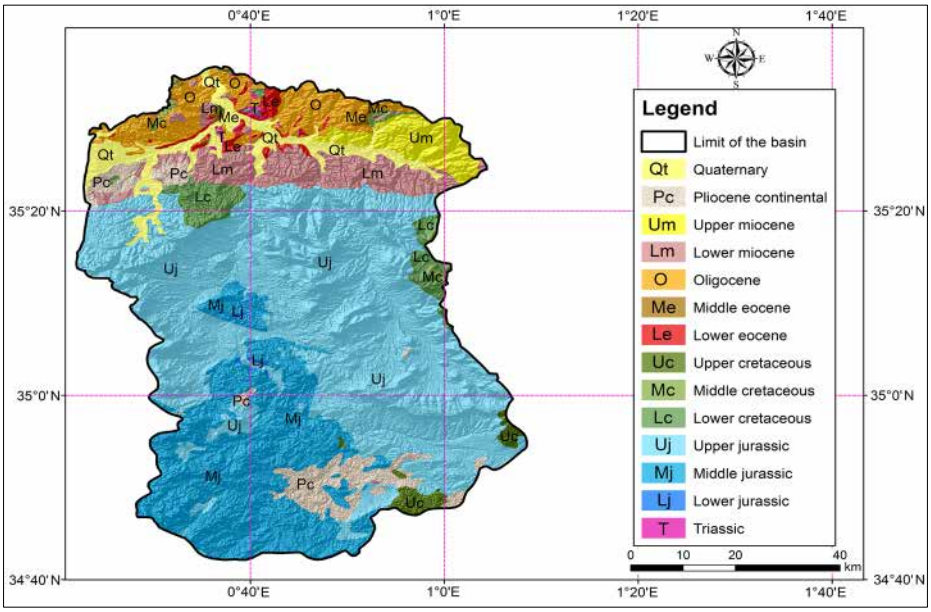

Figure 4. Lithological map of the Wadi Mina basin.

Table 5. Lithology of the Wadi Mina basin at the SMBA.

Era	Area (km^2)	Area (%)
Quaternary	226.01	4.61
Pliocene Continental	225.56	4.60
Upper Miocene	154.21	3.15
Lower Miocene	296.26	6.05
Oligocene	272.32	5.56
Middle Eocene	13.49	0.28
Lower Eocene	52.81	1.08
Upper Cretaceous	53.22	1.09
Lower Cretaceous	136.42	2.78
Middle Cretaceous	115.40	2.36
Upper Jurassic	2341.68	47.79
Middle Jurassic	988.82	20.18
Lower Jurassic	6.86	0.14
Triassic	9.09	0.19
Water	7.84	0.16

The diverse forms of water-induced erosion, sediment conveyance, and reservoir sedimentation observed within the study region are illustrated in Figure 5.

Figure 5. The Wadi Mina basin presents diverse occurrences of hydric erosional phenomena, sedimentary transport, and depositional processes within its dam structures (The photographs were taken at the level of the SMBA impoundment).

3. Materials and Methods

Precipitation is a pivotal factor in driving soil erosion and sediment deposition through various water-mediated erosion processes, encompassing rill erosion, sheet erosion, gully erosion, and splash erosion. The soil particles dislodged by rainfall impact are those that are carried away from a place by the flow [44].

Focusing on the effects of runoff and sheet flow originating from the RUSLE model calculates soil erosion for each pixel.

$$A = R \times K \times LS \times C \times P. \quad (1)$$

The equation describes the yearly soil erosion rate in t ha^{-1} $year^{-1}$ (A), influenced by several critical factors. Rainfall erosivity (R), measured in MJ mm ha^{-1} h^{-1} y^{-1}, reflects the impact of precipitation on erosion. Soil erodibility (K), quantified in t h MJ^{-1} mm^{-1}, represents the susceptibility of the soil to erosion. The dimensionless topographic factor is derived by integrating slope steepness and length (Ls). The cover management factor accounts for the influence of vegetation and ground cover (C), while the dimensionless factor considers the effects of anti-erosion practices and techniques (P).

The RUSLE Model is widely regarded as a practical and effective approach for estimating soil erosion, as it can integrate diverse management strategies while necessitating minimal data inputs. This model is predicated on the principle that soil detachment within a given slope or region is predominantly driven by sediment transport dynamics [45].

Figure 6 depicts the essential stages outlined in the organizational structure for creating a comprehensive soil erosion map.

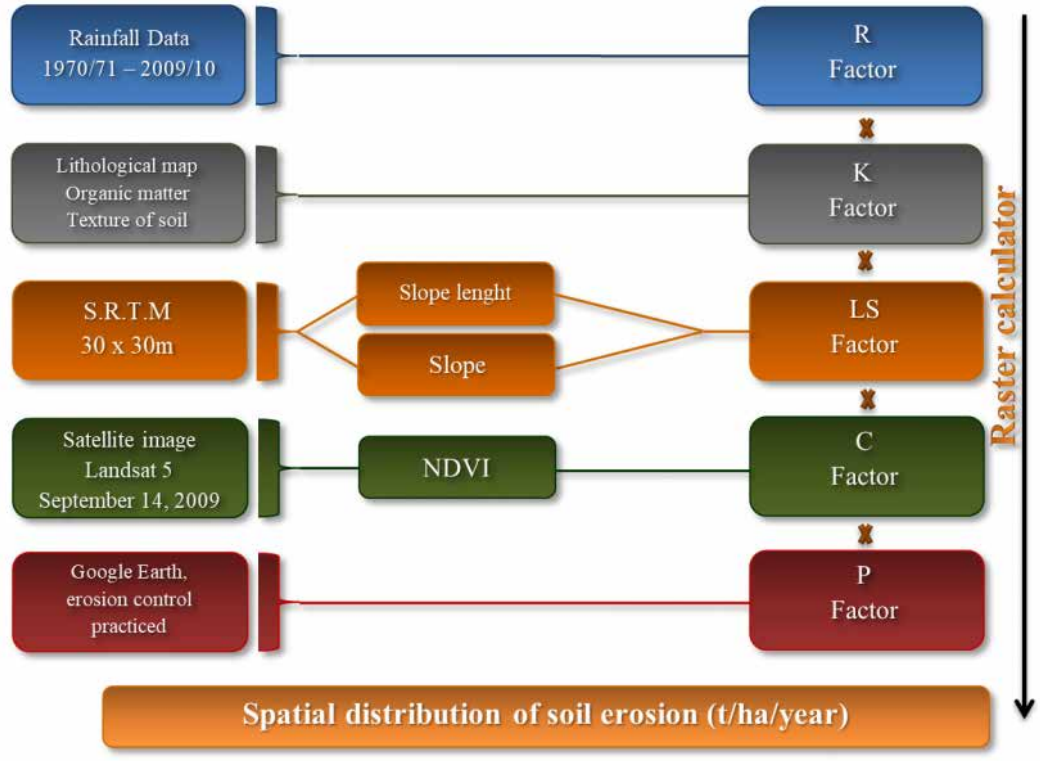

Figure 6. Flowchart of the methodology used in this study.

3.1. Rainfall Erosivity Factor (R)

The R factor provides a quantitative assessment of the erosive capacity of rainfall. The higher the intensity of rainfall, the greater the erosion power, and vice versa. The susceptibility to erosional processes increases in accordance with the magnitude and the

temporal span of rainfall occurrences [46]. In this study, the Diodato [47,48] model was utilized, which estimates R using the following:

$$R = b_0 \cdot P' \cdot \sqrt{d}(\alpha + b_1 \cdot L). \quad (2)$$

In this formulation, b_0 represents a constant value of 0.117 MJ mm ha^{-1} h^{-1}, while b_1 is defined as–0.015 $d^{0.5}$ $mm^{-1.5}$, and the parameter α is expressed as 2.00 $d^{0.5}$ $mm^{-0.5}$. Here, L corresponds to the longitude of the site, P′ denotes the total annual rainfall in millimeters, and d signifies the maximum daily precipitation (in mm d^{-1}) averaged over multiple years. Rainfall monitoring data from 16 stations across the basin were used to calculate R-values, which were then interpolated to produce an R-value map through the Inverse Distance Weighting method (IDW) (Figure 7).

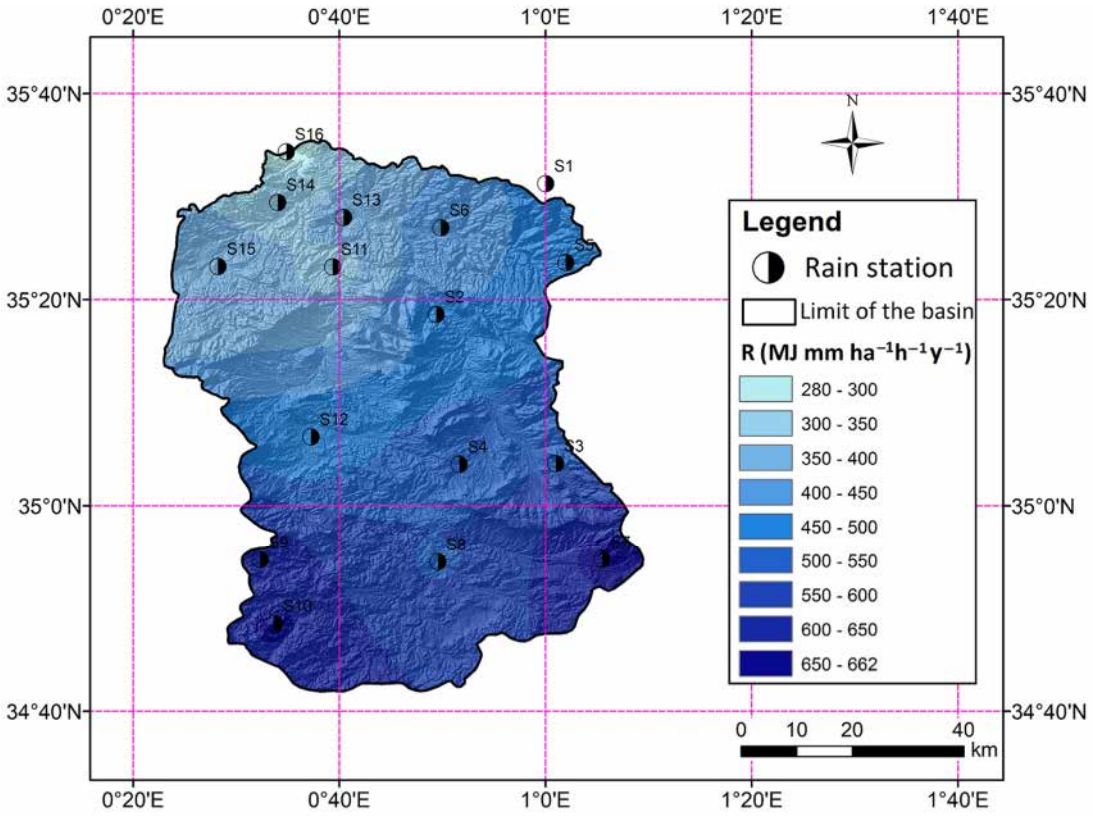

Figure 7. Spatial representation of the rainfall erosivity factor R within the study region.

3.2. Soil Erodibility Factor (K)

The soil's ability to resist erosion, known as the erodibility factor, is influenced by various elements, such as the soil texture, amount of organic matter, structural features, and capacity to absorb water. This factor represents how easily soil particles can be detached and carried away by rainfall or surface water flow [49]. The calculation of the (K) factor is mainly affected by soil texture and organic matter content, as well as by soil structure and permeability [50]. These data are generally extracted from soil cover documents [51], which are not available for the Mina watershed. However, some studies show that there is a relationship between parent rock and texture classification [52] and that soil develops from parent material [53]. For the La Mina watershed, soil texture was deduced from the geological map. All textural classes are identified according to the USDA classification [54]. This allows us to deduce the average percentages of clay, silt and fine sand, and subsequently the values of soil structure (s) and permeability (pr) coefficients.

Soil organic matter (OM) content is linked to vegetation type [55]. Consequently, the relationship between these two parameters (Table 6) allows us to attribute the organic matter rate for the Mina basin [51].

Table 6. Estimated organic matter (OM) content according to land cover.

Large Type	Sub-Type	OM (%)
Cereal and forage farming	undifferentiated	0–0.5
Market gardening (vegetables, tubers)	in the greenhouse	>1.5
	traditional	>1.5
Recent burn	in agricultural zones	0–0.5
	in the Steppic region	0–0.5
	in forested areas	0.5–1.5
	in maquis	0.5–1.5
	undifferentiated	0–0.5
Arboriculture	undifferentiated	>1.5
Forest plantation (undifferentiated)	<50% tree cover	0.5–1.5
	50–75% tree cover	0.5–1.5
	>75% tree cover	>1.5
Deciduous forest plantation	<50% tree cover	0.5–1.5
	50–75% tree cover	0.5–1.5
	>75% tree cover	>1.5
Resinous forest plantation	<50% tree cover	0.5–1.5
	50–75% tree cover	0.5–1.5
	>75% tree cover	>1.5

3.3. Topographic Factor (LS)

The topographic factor is a composite of two subcomponents: the slope gradient factor and the slope length factor. These factors are obtained through a geospatial analysis of the Digital Elevation Model (DEM) [55]. These factors are essential in modeling and understanding surface runoff, also referred to as overland flow, within the context of soil erosion frameworks. The equation formulated by Moore and Burch [56] has been utilized by multiple academic authors, e.g., Markose and Jayappa [46], and was utilized as follows:

$$\mathrm{LS} = \left(\text{flow accumulation} \times \frac{\text{Cell size}}{22.1}\right)^{0.4} \times \left(\sin \text{slope} \times 0.0896\right)^{1.3}. \quad (3)$$

3.4. Cover Management Factor (C)

The cover management factor, also referred to as the C factor, serves to measure the relative rate of soil erosion observed in cultivated fields compared to that of bare, continuously tilled fallow land under analogous environmental conditions. This factor is influenced by several variables, encompassing the characteristics of vegetation cover, the sequence and rotation of crop types, overall agricultural management practices, as well as the timing and intensity of erosive precipitation events throughout the different stages of crop growth [18]. According to Panagos et al. [21] and Mahgoub et al. [57], vegetative ground cover plays a pivotal role in reducing the threat of soil erosion, with its influence second only to that of topographical features [58]. Various methodologies for calculating the C factor have incorporated the Normalized Difference Vegetation Index [59,60]. Reflectance

values were extracted from Landsat satellite imagery to generate the land use map of the study area. These reflectance values were then corrected to adjust for the sun angle. NDVI map was developed by utilizing the red (band 4) and near-infrared (band 5) spectral bands. The corresponding raster layer for the C factor was derived from the NDVI through the following specific computational approach:

$$C = \exp\left[\frac{-\alpha NDVI}{\beta - NDVI}\right]. \quad (4)$$

The variable C represents the plant cover factor, while the Normalized Difference Vegetation Index (NDVI) is calculated using the following formula: NDVI = (R5−R4)/(R5 + R4). Here, α and β are constants with values of 2 and 1, respectively, as outlined by van der Knijff et al. [61].

3.5. Conservation Support Practice Factor (P)

The P factor reflects the impact of surface features on water flow dynamics and hydraulic behavior, encompassing methods like contour farming, strip cropping, and the construction of terraces. By utilizing diverse P factor scenarios, it becomes possible to evaluate how various management strategies influence estimates of soil erosion [18]. In the lack of particular data on conservation techniques in the Mina basin, calculated *p*-values using Morgan's [62] proposal, the proposed approach suggests utilizing *p*-values that vary based on the gradient of the terrain. This methodology is widely applied in research and has been documented extensively in academic literature [21,30].

3.6. Factor of Erosion (A)

RUSLE was applied to estimate soil erosion throughout the Wadi Mina basin. This process required the creation of five distinct raster layers (*.tif), corresponding to the equation's factors: R (rainfall erosivity), K (soil erodibility), LS (topographic factor), C (cover management), and P (support practices). The total soil loss across the study area was determined by multiplying these layers on a pixel-by-pixel basis across the entire basin. (Figure 6).

4. Results and Interpretation

The rainfall erosivity factor was calculated by applying the inverse distance weighting (IDW) method to generate the corresponding spatial map. Erosivity values ranged from 280.0 MJ mm ha^{-1} h^{-1} yr^{-1} at station S16 to 662.90 MJ mm ha^{-1} h^{-1} yr^{-1} at station S7, with an average annual erosivity of 472.78 MJ mm ha^{-1} h^{-1} yr^{-1}. Notably, the southern region of the basin showed significant erosivity (Figure 7). Toubal et al. [30] attributed these observations to four primary factors: (1) the correlation between inter-annual erosivity irregularity and rainfall patterns; (2) the influence of location and precipitation exposure on basin irregularity; (3) spatial variations in wind patterns; and (4) the presence of vegetation cover. The K factor map obtained from the basin shows a variation ranging from 0.0175 to 0.04 t·h·$MJ^{-1}mm^{-1}$ (Figure 8a).

Ranging from 0 to 44.09, the LS factor (Figure 8b) exhibits peak values in the basin's central and northern regions, where exposed, uneven terrain is particularly vulnerable to linear erosion processes.

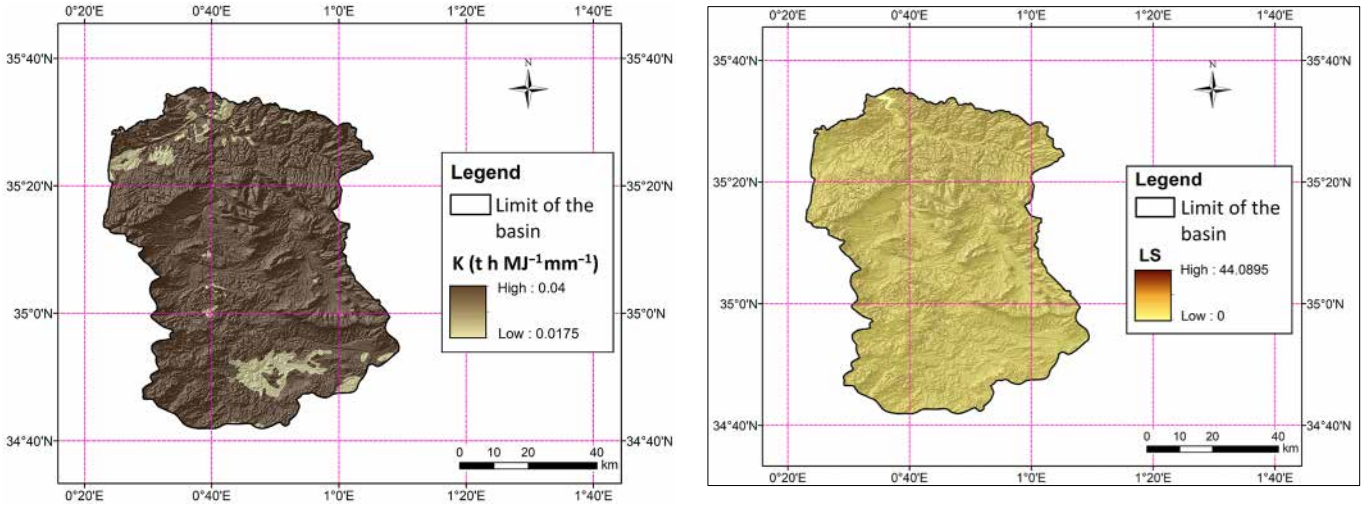

(**a**) (**b**)

Figure 8. Map of the (**a**) K factor and (**b**) topographic factor LS.

The C factor was computed utilizing a spectrum of values spanning from 0.001 to 1.000 (Figure 9), wherein lower values signify enhanced soil protection. Dense vegetative cover serves as a safeguard against soil erosion [37,63].

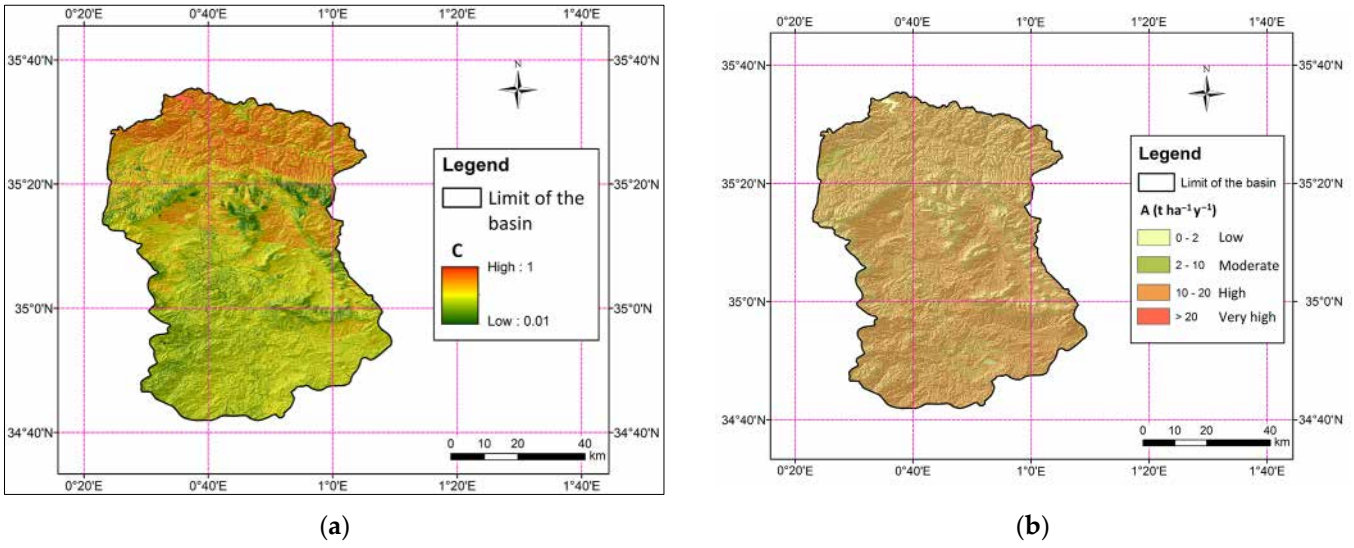

(**a**) (**b**)

Figure 9. Spatiotemporal assessment of the C Factor (**a**) and soil erosion rates (**b**) within the Wadi Mina basin.

Regarding the P factor, given that the majority of the basin lacks erosion control measures, the value P = 1 is predominant. In these regions, soils remain vulnerable to the displacement of splashed particles via surface runoff.

The analysis demonstrates the geographic variation in erosion levels, which span a range from 0 to 772t ha^{-1} yr^{-1} (Figure 9). Within the Wadi Mina basin, erosion risk rates are classified into 7 distinct categories. Notably, the most prevalent class, accounting for 68.8% of the area, falls within the range of 0 to 5 t ha^{-1} yr^{-1} (Figure 10 and Table 7).

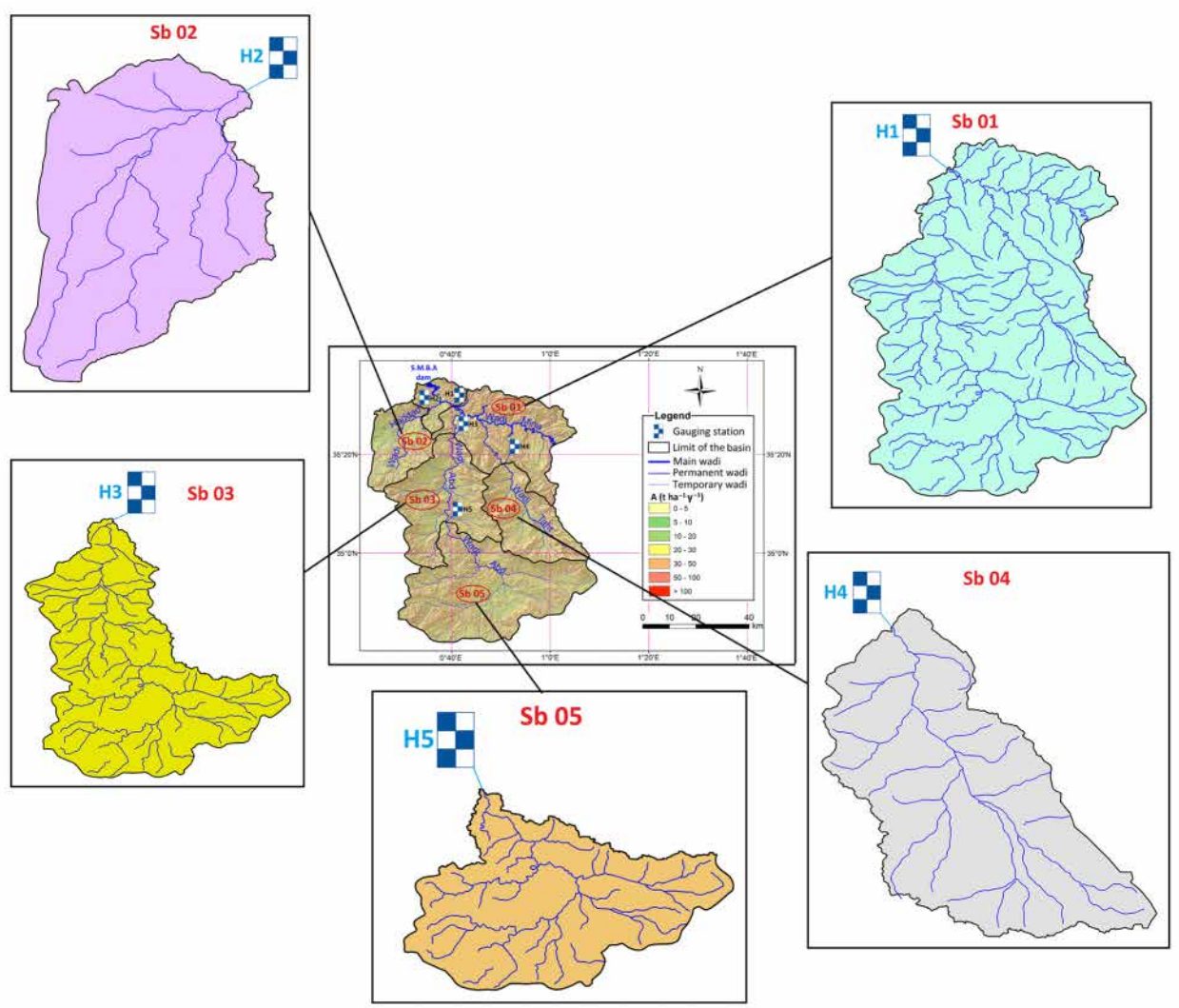

Figure 10. Water erosion variability over the different sub-basins of the wadi Mina basin. The circled numbers represent the sub-basins.

Table 7. Spatial distribution of soil erosion zones.

Categorization of Erosion (t ha^{-1} Year^{-1})	Area (km^2)	Area (%)
0–5	3372.60	68.83
5–10	69.83	1.43
10–20	216.63	4.42
20–30	245.46	5.01
30–50	402.73	8.22
50–100	402.61	8.22
>100	190.14	3.88

Table 8 presents the statistical data for each RUSLE model parameter across the entire basin and its five sub-basins (sub-basin locations depicted in Figure 10). Analysis of the period from 1970/71 to 2009/10 reveals that the basin-wide average erosion rate is 16.69 t ha^{-1} yr^{-1}.

Table 8. Statistics parameters of the different factors of the RUSLE model.

Sub Basin N°	Area (km^2)	Parameter	R (MJ mm ha^{-1} h^{-1} $Year^{-1}$)	K (t h MJ^{-1} mm^{-1})	LS (/)	C (/)	A (t ha^{-1} $Year^{-1}$)
Sub basin 01	4126	Minimum	326.10	0.02	0.00	0.01	0.00
		Maximum	662.90	0.04	44.08	1.00	772.16
		Mean	511.81	0.04	1.40	0.64	17.26
		SD	81.45	0.00	2.98	0.08	35.29
		CV	0.16	0.09	2.12	0.12	2.04
Sub basin 02	480	Minimum	315.25	0.03	0.00	0.00	0.00
		Maximum	421.78	0.04	35.86	1.00	343.61
		Mean	373.74	0.04	1.34	0.63	12.00
		SD	20.69	0.01	2.74	0.09	25.02
		CV	0.06	0.14	2.04	0.14	2.09
Sub basin 03	2480	Minimum	326.10	0.03	0.00	0.01	0.00
		Maximum	662.90	0.04	39.35	1.00	489.39
		Mean	539.11	0.04	1.26	0.62	16.06
		SD	81.48	0.00	2.60	0.07	31.74
		CV	0.15	0.10	2.06	0.11	1.98
Sub basin 04	680	Minimum	447.36	0.03	0.00	0.01	0.00
		Maximum	630.73	0.04	44.09	1.00	772.16
		Mean	522.84	0.04	1.36	0.63	17.36
		SD	40.07	0.00	2.92	0.08	36.21
		CV	0.08	0.02	2.15	0.12	2.09
Sub basin 05	1553	Minimum	456.49	0.03	0.00	0.01	0.00
		Maximum	662.90	0.04	35.75	1.00	489.39
		Mean	590.98	0.04	1.12	0.63	15.82
		SD	39.22	0.00	2.10	0.06	29.74
		CV	0.07	0.13	1.88	0.10	1.88
Entire basin	4900	Minimum	280.02	0.02	0.00	0.01	0.00
		Maximum	662.90	0.04	44.08	1.00	772.16
		Mean	490.94	0.04	1.41	0.64	16.69
		SD	92.46	0.00	2.99	0.08	34.33
		CV	0.19	0.08	2.12	0.12	2.06

Achite et al. [64] proposed a method for quantifying the suspended sediment yield (SSY) at a daily scale for each sub-basin, employing sediment rating curves (SRC) and river discharge time series over the period from 1970/71 to 2009/10 (Table 8).

Assuming that the SSY values and gross erosion estimates provided for 1970–2010 in this study accurately represent the current conditions of the Upper Mina basin and are comparable, the analysis provides the following results. At the Wadi Abtal station, the RUSLE model estimates a specific soil loss of 17.26 t ha^{-1} $year^{-1}$ (or 1726 t km^{-2} $year^{-1}$), while the specific suspended sediment yield is 271.45 t km^{-2} $year^{-1}$.

This translates into a Sediment Delivery Ratio (SDR) of 15.73% (Table 9). The same analytical approach was applied to evaluate the other sub-basins and the entire basin. Analysis of the Sediment Delivery Ratio (SDR) reveals significant variation across different basins. The Wadi Taht basin at Kef Mehboula station exhibits a low SDR of 5.50%, while the Wadi Haddad basin at Sidi Abdelkader Djillali station demonstrates a markedly higher SDR of 81.27%. Notably, the Oued Haddad basin displays an elevated average specific load in comparison to other sub-basins, contributing to its substantially high SDR. This phenomenon can be attributed to the basin's unique characteristics, including its topographical features and temporally and spatially variable vegetation cover, which render it particularly susceptible to peak flow events or flooding [64,65].

Table 9. Average sediment yield values estimated in tributary sub-basins of the Wadi Mina basin and gross erosion values over 1970–2010.

Sub-Basin	Wadi	Area (km^2)	SRC	SSY ($t\ km^{-2}\ yr^{-1}$) for 1970–2010	RUSLE ($t\ ha^{-1}\ yr^{-1}$) for 1970–2010	SDR (%)
Sub basin 01	Upstream Mina	4126	$Qs = 3.50Ql^{1.38}$	271.45	17.26	15.73
Sub basin 02	Haddad	480	$Qs = 3.48Ql^{1.38}$	975.45	12.00	81.27
Sub basin 03	Abd	2480	$Qs = 2.27Ql^{1.65}$	227.42	16.06	14.13
Sub basin 04	Taht	680	$Qs = 5.32Ql^{1.41}$	95.62	17.36	5.50
Sub basin 05	Abd	1553	$Qs = 4.23Ql^{1.46}$	105.20	15.82	6.64
Entire	Mina	4900		320.41	16.69	19.20

As regards the dimensions of the sub-basins shown in Tables 8 and 9, it should be noted that each hydrometric station represents the outlet of the sub-basin considered. Each hydrometric station monitors the waters of the drainage surfaces of each sub-basin. Of the five sub-basins, four have common drainage surfaces; only the sub-basin of Wadi Haddad at the Sidi Abdelkader Djillali station has a drainage surface isolated from the others.

In recent decades, the prioritization of basins has undergone a paradigm shift, largely attributed to the advancements in remote sensing and GIS technologies [66–68]. The integration of decision support systems, exemplified by the analytic hierarchy process (AHP) [69–71], alongside cutting-edge data-driven approaches such as machine learning methodologies, has proven instrumental in modeling environmental and natural resource dynamics. Sub-basins, characterized by their heterogeneous spatial attributes, including topography, soil composition, land use patterns, and geomorphological features, require systematic prioritization. This process is crucial for identifying areas that demand immediate conservation interventions, ultimately aimed at enhancing the overall condition of natural resources and the environment.

In this context, the priority for action is the development of a water and soil conservation action plan for the basin. To accomplish this, an automated division was performed based on the digital terrain model of the study area. This process ultimately delineated 28 sub-basins (Figure 11) starting from the division already drawn up by the national water resources agency (ANRH). The sub-basins of study areas 9, 6, 7, 8, 24, 26, 27, and 28 are the most critical for development due to their proximity to the dam, estimated at 10 km, and their average rates of soil loss, estimated at 22.39, 11.48, 12.25, 15.77, 21.39, 16.67, 13.00, and 16.20 t/ha/year, respectively. For the highest intervention priority, an area of 223.24 km^2 of land highly susceptible to erosion requires development. Nine sub-basins have been classified as high priority, with average soil losses ranging from 11.48 to 22.39 $t\ ha^{-1}\ yr^{-1}$. These are predominantly located in the northern part of the catchment (Figure 11 and Table 10).

For anyone aiming to model erosion, it is essential that simulations can be validated. However, in many instances, particularly in semi-arid regions where economic activity is limited, local authorities often lack the resources to carry out such validation. In these cases, models are primarily used as tools for spatializing information to identify areas most vulnerable to erosion. This serves various purposes: conservation planning, guiding public policy, and prioritizing actions to mitigate soil degradation. In this context, while full validation of the models is not feasible, the order of magnitude of the results can be cross-checked using the limited available data, specifically solid transport measurements from hydrological stations. Using the RUSLE model, the average annual erosion potential for the entire river basin is estimated at 16.7 tons per hectare, corresponding to a Sediment

Delivery Ratio (SDR) of 19%. This estimate aligns well with general SDR values reported in major studies, which range from 13% to 40% [72].

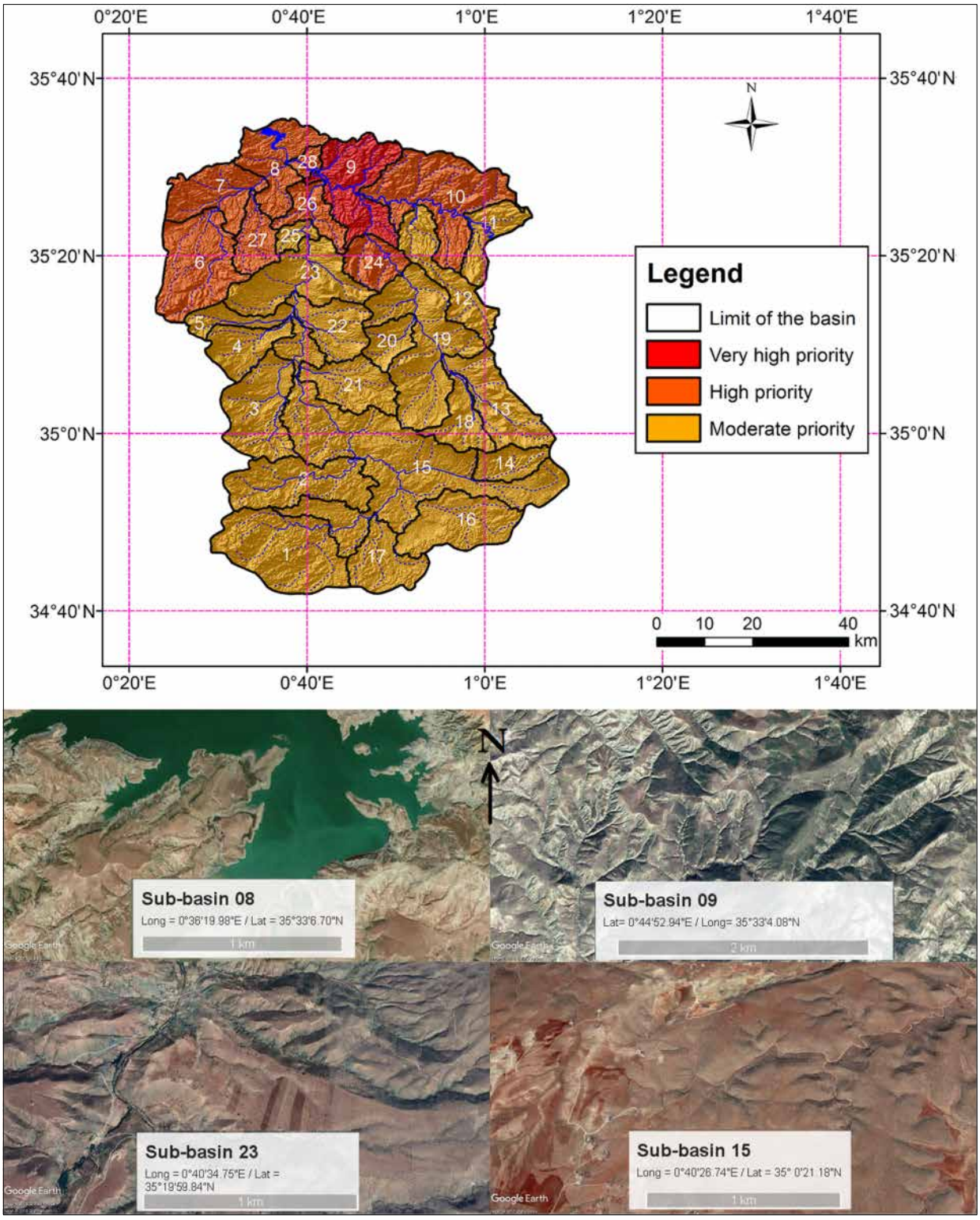

Figure 11. A priority map delineating the sub-basin of the Wadi Mina basin and the spatial characterization of diverse forms of water erosion.

Table 10. Priority of intervention by sub-basin of the study area.

Sub-Basin	Area (km^2)	A (t ha^{-1} yr^{-1})	Distance to the Dam (km)	Intervention Priority
1	305.70	17.03	100.33	Moderate
2	231.70	16.20	67.88	Moderate
3	213.79	16.50	41.60	Moderate
4	115.23	15.47	28.80	Moderate
5	129.62	17.79	26.40	Moderate
6	249.10	11.48	19.32	High
7	160.76	12.25	7.50	High
8	173.95	15.77	0.00	High
9	223.24	22.10	9.10	Very High
10	315.16	21.08	25.18	High
11	102.85	17.39	54.08	Moderate
12	164.75	19.87	37.98	Moderate
13	184.01	17.84	71.60	Moderate
14	83.56	19.03	92.14	Moderate
15	610.44	15.37	42.50	Moderate
16	216.00	14.78	86.38	Moderate
17	129.36	14.47	88.13	Moderate
18	93.72	16.07	76.10	Moderate
19	334.55	17.29	49.10	Moderate
20	66.43	18.39	61.04	Moderate
21	137.20	15.39	37.66	Moderate
22	124.23	15.84	47.63	Moderate
23	222.37	16.84	32.55	Moderate
24	90.34	21.39	36.50	High
25	32.52	18.62	27.09	Moderate
26	81.00	16.67	14.00	High
27	84.23	13.00	11.20	High
28	24.20	16.20	2.10	High
Sum	4900.0			

5. Conclusions and Recommendations

The present study aimed to develop a spatial distribution map of water erosion risk in Northwestern Algeria by integrating the RUSLE model, remote sensing, and geographic information systems. This approach incorporated the assessment of five key components: R, LS, C, K, and P. Findings from the study reveal that the RUSLE model-derived specific soil loss in Wadi Mina at Oued Abtal station amounts to 17.26 t ha^{-1} yr^{-1}. For the sub-basins of Wadi Haddad (Sidi Abdelkader Djillali station), Wadi Abd (Ain Ammara station), Wadi That (Kef Mehboula station), and Wadi Abd (Takhmaret Station), the observed erosion rates are 12, 16.06, 17.36, and 15.82 t ha^{-1} yr^{-1}, respectively. The Wadi Mina basin at the SMBA exhibits an average annual erosion rate of approximately 16.69 t ha^{-1} yr^{-1}. Analysis of GIS-generated maps for various criteria indicates that the northern regions of the basin demonstrate the highest susceptibility to erosion. The RUSLE model proves valuable in providing extensive insights into the erosion process and spatially delineating erosion-prone areas within the basin. While these data offer relative values, they serve as crucial tools for analyzing potential erosion rates, identifying factors contributing to land

degradation, developing evolution scenarios, and pinpointing priority areas that require immediate conservation interventions and erosion mitigation measures.

Author Contributions: Conceptualization, M.A.; methodology, A.K.T.; software, M.A. and A.K.T.; validation, M.A. and A.K.T.; formal analysis, M.A.; investigation, P.C. and T.C.; data curation, M.A.; writing—original draft preparation, M.A.; writing—review and editing, M.A., P.C., T.C., A.D.M. and S.O.; visualization, M.A. and A.K.T.; supervision, S.O. All authors have read and agreed to the published version of the manuscript.

Funding: This research received no external funding.

Institutional Review Board Statement: Not applicable.

Informed Consent Statement: Not applicable.

Data Availability Statement: The datasets used and/or analyzed during the current study are available from the corresponding author on reasonable request.

Acknowledgments: We thank the National Agency of Water Resources (ANRH) for the collected data and the General Directorate of Scientific Research and Technological Development of Algeria (DGRSDT).

Conflicts of Interest: The authors declare no conflicts of interest.

Abbreviations

The following abbreviations are used in this manuscript:

RUSLE	Revised Universal Soil Loss Equation
R	erosive capacity of rainfall
K	susceptibility of soil to erosion
Ls	length and gradient of slopes
C	characteristics of cover management
P	conservation measures
SDR	Sediment Delivery Ratio
DEM	Digital Elevation Model
ANRH	National Water Resources Agency
SRTM	Shuttle Radar Topographic Mission
USGS	United States Geological Survey
SSY	suspended sediment yield
SRC	sediment rating curves

References

1. Chadli, K. Estimation of soil loss using RUSLE model for Sebou watershed (Morocco). *Model. Earth Syst. Environ.* **2016**, *2*, 51. [CrossRef]
2. Igwe, P.U.; Onuigbo, A.A.; Chinedu, O.C.; Ezeaku, I.I.; Muoneke, M.M. Soil erosion: A review of models and applications. *Int. J. Adv. Sci. Res.* **2017**, *4*, 138–150. [CrossRef]
3. Wischmeier, W.H.; Smith, D.D. *Predicting Rainfall Erosion Losses, a Guide to Conservation Planning*; U.S. Department of Agriculture: Washington, DC, USA, 1978; Volume 537, p. 62.
4. Renard, K.G.; Foster, G.R.; Weesies, G.A.; Porter, J.P. RUSLE: Revised universal soil loss equation. *J. Soil Water Conserv.* **1991**, *46*, 30–33. [CrossRef]
5. Morgan, R.P.C.; Quinton, J.N.; Smith, R.E.; Govers, G.; Poesen, J.W.A.; Auerswald, K.; Chisci, G.; Torri, D.; Styczen, M.E. The European soil erosion model (EUROSEM): A dynamic approach for predicting sediment transport from felds and small catchments. *Earth Surf. Process. Landf.* **1998**, *23*, 527–544. [CrossRef]
6. Gavrilovic, S. *Engineering of Debris Flow and Erosion*; Izgradnja: Belgrade, Serbia, 1972; p. 292. (In Serbian)
7. De Roo, A.P.J.; Hazelhoff, L.; Burrough, P.A. Soil erosion modelling using 'answers' and geographical information systems. *Earth Surf. Process. Landf.* **1989**, *14*, 517–532. [CrossRef]

8. Loch, R.J.; Silburn, D.M.; Freebairn, D.M. Evaluation of the CREAMS model II. Use of rainulator data to derive soil erodibility parameters and prediction of field soil losses using derived parameters. *Aust. J. Soil Res.* **1989**, *27*, 563–576. [CrossRef]
9. Smith, R.E.; Goodrich, D.C.; Quinton, J.N. Dynamic, distributed simulation of watershed erosion: The KINEROS2 and EUROSEM models. *J. Soil Water Conserv.* **1995**, *50*, 517–520. [CrossRef]
10. Botterweg, P.; Leek, R.; Romstad, E.; Vatn, A. The EUROSEMGRIDSEM modelling system for erosion analyses under different natural and economic conditions. *Ecol. Model.* **1998**, *108*, 115–129. [CrossRef]
11. Williams, J.R.; Jones, C.A.; Dyke, P.T. A modeling approach to determining the relationship between erosion and soil productivity. *Trans. ASAE* **1984**, *27*, 129–144. [CrossRef]
12. De Jong van Lier, Q.; Sparovek, G.; Flanagan, D.C.; Bloem, E.M.; Schnug, E. Runoff mapping using WEPP erosion model and GIS tools. *Comput. Geosci.* **2005**, *31*, 1270–1276. [CrossRef]
13. Kirkby, M.J.; Le Bissonais, Y.; Coulthard, T.J.; Daroussin, J.; McMahon, M.D. The development of land quality indicators for soil degradation by water erosion. *Agric. Ecosyst. Environ.* **2000**, *81*, 125–135. [CrossRef]
14. Srinivasan, R.; Engel, B.A. A spatial decision support system for assessing agricultural nonpoint source pollution. *Water Resour. Bull.* **1994**, *30*, 441–452. [CrossRef]
15. Viney, N.R.; Sivapalan, M.; Deeley, D. A conceptual model of nutrient mobilisation and transport applicable at large catchment scales. *J. Hydrol.* **2000**, *240*, 23–44. [CrossRef]
16. Arnold, J.G.; Srinivasan, R.; Muttiah, R.S.; Williams, J.R. Large area hydrologic modeling and assessment part I: Model development. *J. Am. Water Resour. Assoc.* **1998**, *34*, 73–89. [CrossRef]
17. De Vente, J.; Poesen, J.; Verstraeten, G.; Govers, G.; Vanmaercke, M.; van Rompaey, A.; Arabkhedri, M.; Boix-Fayos, C. Predicting soil erosion and sediment yield at regional scales: Where do we stand? *Earth-Sci. Rev.* **2013**, *127*, 16–29. [CrossRef]
18. Dutta, S. Soil erosion, sediment yield and sedimentation of reservoir: A review. *Model. Earth Syst. Environ.* **2016**, *2*, 123. [CrossRef]
19. Batista, P.V.G.; Davies, J.; Silva, M.L.N.; Quinton, J.N. On the evaluation of soil erosion models: Are we doing enough? *Earth-Sci. Rev.* **2019**, *197*, 102898. [CrossRef]
20. Azaiez, N. Quantification des pertes en terre dans le bassin versant de l'oued Chaâf au Sud-Ouest de l'Arabie Saoudite. *Cinq Cont.* **2024**, *14*, 74–97.
21. Panagos, P.; Borrelli, P.; Meusburger, K.; Alewell, C.; Lugato, E.; Montanarella, L. Estimating the soil erosion cover-management factor at the European scale. *Land Use Policy* **2015**, *48*, 38–50. [CrossRef]
22. Terranova, O.; Antronico, L.; Coscarelli, R.; Iaquinta, P. Soil erosion risk scenarios in the Mediterranean environment using RUSLE and GIS: An application model for Calabria (southern Italy). *Geomorphology* **2009**, *112*, 228–245. [CrossRef]
23. Onori, F.; De Bonis, P.; Grauso, S. Soil erosion prediction at the basin scale using the revised universal soil loss equation (RUSLE) in a catchment of Sicily (southern Italy). *Environ. Earth Sci.* **2006**, *50*, 1129–1140. [CrossRef]
24. Balasubramani, K.; Veena, M.; Kumaraswamy, K.; Saravanabavan, V. Estimation of soil erosion in a semi-arid watershed of Tamil Nadu (India) using revised universal soil loss equation (rusle) model through GIS. Model. *Earth Syst. Environ.* **2015**, *1*, 10. [CrossRef]
25. Kefi, M.; Yoshino, K.; Setiawan, Y.; Zayani, K.; Boufaroua, M. Assessment of the effects of vegetation on soil erosion risk by water: A case of study of the Batta watershed in Tunisia. *Environ. Earth Sci.* **2011**, *64*, 707–719. [CrossRef]
26. Chafai, A.; Brahim, N.; Shimi, N.S. Mapping of water erosion by GIS/RUSLE approach: Watershed Ayda river—Tunisia study. *Arab. J. Geosci.* **2020**, *13*, 810. [CrossRef]
27. Brahim, B.; Meshram, S.G.; Abdallah, D.; Larbi, B.; Drisss, S.; Khalid, M.; Khedher, K.M. Mapping of soil sensitivity to water erosion by RUSLE model: Case of the Inaouene watershed (Northeast Morocco). *Arab. J. Geosci.* **2020**, *13*, 1153. [CrossRef]
28. Ed-daoudy, L.; Lahmam, N.; Benmansour, M.; Afilal, H.; Ben Harra, A.; Damnati, B. Hydric erosion rates in Raouz watershed, Morocco: RUSLE, GIS, and remote sensing. *RSASE* **2023**, *32*, 101056. [CrossRef]
29. Benchettouh, A.; Kouri, L.; Jebari, S. Spatial estimation of soil erosion risk using RUSLE/GIS techniques and practices conservation suggested for reducing soil erosion in Wadi Mina watershed (northwest, Algeria). *Arab. J. Geosci.* **2017**, *10*, 79. [CrossRef]
30. Toubal, A.K.; Achite, M.; Ouillon, S.; Dehni, A. Soil erodibility mapping using the RUSLE model to prioritize erosion control in the Wadi Sahouat basin, North-West of Algeria. *Environ. Monit. Assess.* **2018**, *190*, 210. [CrossRef]
31. Djoukbala, O.; Hasbaia, M.; Benselama, O.; Mazour, M. Comparison of the erosion prediction models from USLE, MUSLE and RUSLE in a Mediterranean watershed, case of Wadi Gazouana (NW of Algeria). *Model. Earth Syst. Environ.* **2019**, *5*, 725–743. [CrossRef]
32. Chikh, H.; Habi, M.; Morsli, B. Influence of vegetation cover on the assessment of erosion and erosive potential in the Isser marly watershed in northwestern Algeria—Comparative study of RUSLE and PAP/RAC methods. *Arab. J. Geosci.* **2019**, *12*, 154. [CrossRef]
33. Sahli, Y.; Mokhtari, E.; Merzouk, B.; Laignel, B.; Vial, C.; Madani, K. Mapping surface water erosion potential in the Soummam watershed in Northeast Algeria with RUSLE model. *J. Mt. Sci.* **2019**, *16*, 1606–1615. [CrossRef]

34. Badreddine, B.; Mohammed, H.; Boutkhil, M.; Ahmed, A. Assessment of erosion: Use of nuclear techniques and conventional methods—Case of the Fergoug watershed, Algeria. *Environ. Monit. Assess.* **2021**, *193*, 55. [CrossRef] [PubMed]
35. Bouamrane, A.; Bouamrane, A.; Abida, H. Water erosion hazard distribution under a Semi-arid climate Condition: Case of Mellah Watershed, North-eastern Algeria. *Geoderma* **2021**, *403*, 115381. [CrossRef]
36. Ouadja, A.; Benfetta, H.; Porto, P.; Flanagan, D.C.; Mihoubi, M.K.; Omeir, M.R.; Graia, M.; Ghosal, K.; Talchabhadel, R. Mapping potential soil erosion using RUSLE, Remote Sensing, and GIS: A case study in the watershed of Oued El Ardjem, Northwest Algeria. *Arab. J. Geosci.* **2021**, *14*, 1945. [CrossRef]
37. Boussadia-Omari, L.; Ouillon, S.; Hirche, A.; Salamani, M.; Guettouche, M.S.; Ihaddadene, L.; Nedjraoui, D. Contribution of phytoecological data to spatialize soil erosion: Application of the RUSLE model in the Algerian Atlas. *ISWCR* **2021**, *9*, 502–519. [CrossRef]
38. Bensekhria, A.; Bouhata, R. Assessment and Mapping Soil Water Erosion Using RUSLE Approach and GIS Tools: Case of Oued el-Hai Watershed, Aurès West, Northeastern of Algeria. *ISPRS Int. J. Geo-Inf.* **2022**, *11*, 84. [CrossRef]
39. Saoud, M.; Meddi, M. Estimation of soil erosion and sediment yield in Wadi El Hachem watershed (Algeria) using the RUSLE-SDR approach. *J. Mt. Sci.* **2023**, *20*, 367–380. [CrossRef]
40. Benchettouh, A.; Jebari, S.; Kouri, L. Spatial Estimation of Soil Erosion Risk Using RUSLE/GIS Techniques and Practices Conservation Suggested for Reducing Soil Erosion in Wadi Mina Catchment (Northwest, Algeria). In *Soil Erosion—Current Challenges and Future Perspectives in a Changing World*; Vieira, A., Carlos Rodrigues, S., Eds.; IntechOpen: London, UK, 2021. [CrossRef]
41. Achite, M.; Meddi, M. Variabilité spatio-temporelle des apports liquide et solide en zone semi-aride. Cas du bassin versant de l'oued Mina (nord-ouest algérien). *Rev. Sci. l'Eau/J. Water Sci.* **2005**, *18*, 37–56. [CrossRef]
42. Hallouz, F.; Meddi, M.; Mahé, G.; Toumi, S.; Ali Rahmani, S.E. Erosion, Suspended Sediment Transport and Sedimentation on the Wadi Mina at the Sidi M'Hamed Ben Aouda Dam, Algeria. *Water* **2018**, *10*, 895. [CrossRef]
43. Achite, M.; Touaibia, B. Sécheresse et gestion des ressources en eau dans le bassin versant de la Mina. In Proceedings of the Algérie 2ème Colloque International sur l'Eau et l'Environnement, Sidi Fredj, Algeria, 30–31 January 2007.
44. Biswas, S.S.; Pani, P. Estimation of soil erosion using RUSLE and GIS techniques: A case study of Barakar River basin, Jharkhand, India. *Model. Earth Syst. Environ.* **2015**, *1*, 42. [CrossRef]
45. Ganasiri, B.P.; Ramesh, H. Assessment of soil erosion by RUSLE model using remote sensing and GIS—A case study of Nethravathi Basin. *Geosci. Front.* **2016**, *7*, 953–961. [CrossRef]
46. Markose, V.J.; Jayappa, K.S. Soil loss estimation and prioritization of sub-watersheds of Kali River basin, Karnataka, India, using RUSLE and GIS. *Environ. Monit. Assess.* **2016**, *188*, 225. [CrossRef] [PubMed]
47. Diodato, N. Estimating Rusle's rainfall factor in the part of Italy with a Mediterranean rainfall regime. *J. Hydrol. Earth Syst. Sci.* **2004**, *48*, 103–107. [CrossRef]
48. Diodato, N. Geostatistical uncertainty modelling for the environmental hazard assessment during single erosive rainstorm events. *Environ. Monit. Assess.* **2005**, *105*, 25–42. [CrossRef]
49. Sekyi-Annan, E.; Gaisie, E.; Issaka, R.N.; Quansah, G.W.; Adams, S.; Bessah, E. Estimating Soil Loss for Sustainable Crop Production in the Semi-deciduous Forest Zone of Ghana. *Front. Sustain. Food Syst.* **2021**, *5*, 674–816. [CrossRef]
50. Lee, E.; Ahn, S.; Im, S. Estimation of soil erosion rate in the Democratic People's Republic of Korea using the RUSLE model. *For. Sci. Technol.* **2017**, *13*, 100–108. [CrossRef]
51. Tecsult. *Étude de la Protection des Bassins Versants de Sidi-Yacoub. Phase, I*; Agence Nationale des Barrages et Transferts: Kouba, Algeria, 2006; 161p.
52. Shirazi, M.A.; Boersma, L.; Johnson, C.B. Particle-Size Distributions. *Soil Sci. Soc. Am. J.* **2001**, *65*, 300. [CrossRef]
53. Olson, K.R. Factors of soil formation | parent material. In *Encyclopedia of Soils in the Environment*; Elsevier: Amsterdam, The Netherlands, 2005; pp. 532–535. [CrossRef]
54. Morsli, B.; Mazour, M.; Mededjel, N.; Hamoudi, A.; Roose, E. Influence de l'utilisation des terres sur les risques de ruissellement et d'érosion sur les versants semi-arides du nord-ouest de l'Algérie. *Sci. Change Planét/Sécher.* **2004**, *15*, 96–104.
55. Budhathoki, S.; Poudel, A.H.L. Soil Erosion Analysis Using GIS and RS in Makawanpur District, Nepal. *J. For. Nat. Resour. Manag.* **2023**, *23*, 68–81. [CrossRef]
56. Moore, I.D.; Burch, G.J. Physical basis of the length-slope factor in the Universal Soil Loss Equation. *Soil Sci. Soc. Am. J.* **1986**, *50*, 1294–1298. [CrossRef]
57. Mahgoub, M.; Elalfy, E.; Soussa, H.; Abdelmonem, Y. Relation between the soil erosion cover management factor and vegetation index in semi-arid basins. *Environ. Earth Sci.* **2024**, *83*, 337. [CrossRef]
58. Mazahreh, S.; Bsoul, M.; Hamoor, D.A. GIS Approach for Assessment of Land Suitability for Different Land Use Alternatives in Semi Arid Environment in Jordan: Case Study (Al Gadeer Alabyad-Mafraq). *Inf. Process. Agric.* **2019**, *6*, 91–108. [CrossRef]
59. Lin, C.Y.; Lin, W.T.; Chou, W.C. Soil erosion prediction and sediment yield estimation: The Taiwan experience. *Soil Tillage Res.* **2002**, *68*, 143–152. [CrossRef]

60. Wang, G.; Wente, S.; Gertner, G.Z.; Anderson, A. Improvement in mapping vegetation cover factor for the universal soil loss equation by geostatistical methods with landsat thematic mapper images. *Int. J. Remote Sens.* **2002**, *23*, 3649–3667. [CrossRef]
61. Van der Knijff, J.M.; Jones, R.J.A.; Montanarella, L. *Soil Erosion Risk Assessment in Europe*; European Commission, European Soil Bureau: Luxembourg, 2000; p. 44.
62. Morgan, R.P.C. A simple approach to soil loss prediction: A revised Morgan–Morgan–Finney model. *Catena* **2001**, *44*, 305–322. [CrossRef]
63. Almohamad, H. Impact of Land Cover Change Due to Armed Conflicts on Soil Erosion in the Basin of the Northern Al-Kabeer River in Syria Using the RUSLE Model. *Water* **2020**, *12*, 3323. [CrossRef]
64. Achite, M.; Toubal, K.A.; Katipoğlu, O.M.; Elshaboury, N. Comparative study of different estimation approaches to quantify suspended sediment transport at hydrometric stations: Case of the wadi Mina basin, Northwest Algeria. *Int. J. Energy Water Resour.* **2024**, *9*, 421–433. [CrossRef]
65. Achite, M.; Ouillon, S. Recent changes in climate, hydrology and sediment load in the Wadi Abd, Algeria (1970–2010). *Hydrol. Earth Syst. Sci.* **2016**, *20*, 1355–1372. [CrossRef]
66. Chen, W.; Xie, X.; Wang, J.; Pradhan, B.; Hong, H.; Bui, D.T.; Duan, Z.; Ma, J. A comparative study of logistic model tree, random forest, and classification and regression tree models for spatial prediction of landslide susceptibility. *Catena* **2017**, *151*, 147–160. [CrossRef]
67. Mundetia, N.; Sharma, D.; Dubey, S.K. Morphometric assessment and sub-watershed prioritization of Khari River basin in semi-arid region of Rajasthan India. *Arab. J. Geosci.* **2018**, *11*, 530. [CrossRef]
68. Wu, H. Watershed prioritization in the upper Han River basin for soil and water conservation in the South-to-North Water Transfer Project (middle route) of China. *Environ. Sci. Pollut. Res.* **2018**, *25*, 2231–2238. [CrossRef] [PubMed]
69. Randhir, T.; Shriver, D.M. Deliberative valuation without prices: A multiattribute prioritization for watershed ecosystem management. *Ecol. Econ.* **2009**, *68*, 3042–3051. [CrossRef]
70. Chowdary, V.M.; Chakraborthy, D.; Jeyaram, A.; Murthy, Y.V.N.K.; Sharma, J.R.; Dadhwal, V.K. Multi-criteria decision making approach for watershed prioritization using analytic hierarchy process technique and GIS. *Water Resour. Manag.* **2013**, *27*, 3555–3571. [CrossRef]
71. Jaiswal, R.K.; Thomas, T.; Galkate, R.V.; Ghosh, N.C.; Singh, S. Watershed prioritization using Saaty's AHP based decision support for soil conservation measures. *Water Resour. Manag.* **2014**, *28*, 475–494. [CrossRef]
72. Ouillon, S. Why and How Do We Study Sediment Transport? Focus on Coastal Zones and Ongoing Methods. *Water* **2018**, *10*, 390. [CrossRef]